Solid State Tuning of TiO_2 Morphology, Crystal Phase and Size through Metal Macromolecular Complexes and its Significance in the Photocatalytic Response

Patricio Allende-González[1], Miguel Ángel Laguna-Bercero[2], Lorena Barrientos*[3], María Luisa Valenzuela[4] and Carlos Díaz*[1]

*1. Departamento de Química, Facultad de Ciencias, Universidad de Chile. La Palmeras 3425, Ñuñoa, casilla 653, Santiago de Chile, 7800003, Chile. *Corresponding author E-mail: cdiaz@uchile.cl*

2. Instituto de Ciencia de Materiales de Aragón, ICMA, CSIC-Universidad de Zaragoza, María de Luna 3, 50018 – Zaragoza, Spain.

*3. Facultad de Química, Centro de Investigación en Nanotecnología y Materiales Avanzados CIEN-UC, Pontificia Universidad Católica de Chile, Vicuña Mackenna 4860, Macul, Santiago de Chile, Chile. *Corresponding author E-mail: lbarrientop@uc.cl*

4. Universidad Autónoma de Chile, Institute of Applied Chemical Sciences, Inorganic Chemistry and Molecular Materials Group, El Llano Subercaseaux 2801, 5° piso, San Miguel, Santiago, Chile.

Abstract

A solid-state phase control of TiO_2 by the use of different macromolecular complex precursors is reported for the first time. During the formation of TiO_2 nanoparticles, chitosan and Poly(styrene-co-4-vinylpyridine) polymers can act as solid-state template producing areas after carbonization, where the TiO_2 nucleates. It seems that the location of metal centers through the polymeric chain (i.e. the distance between the metal centers) strongly influence the morphology and particle size of the photocatalyst. To demonstrate the application value of our different TiO_2 structures, the photocatalytic behavior was explored. The efficient photocatalytic decoloration of methylene blue on different polymorphic forms of nanostructured TiO_2 is confirmed. The best photocatalyst achieved 98% of discoloration rate in only 25 min when the pH of the solution is 9.5, improving the efficiency of the standard photocatalyst Degussa P25 without the addition of other phases or dopants. The novelty of the present work is that by means of an appropriate synthesis, can be tuned simultaneously the three main factors (morphology, size and crystalline phase) that allow modulating the photocatalytic response of titania material. This control has allowed an advance in the properties of the material, managing to increase the photo-response in a short time.

Keywords: TiO_2 nanoparticles, Photocatalysis, solid-state synthesis, morphology, size and crystal phase.

1. INTRODUCTION

Organic pollutants have become one of the most serious environmental problems nowadays, due to their high toxicity and difficulty to be degraded.[1-4] In this respect, the use of nanomaterials such as metal oxide in Advanced Oxidation Processes (AOPs) has attracted increased attention owing to their unique physical and chemical characteristics, and therefore its effectiveness as pollutant removal. Among all the semiconductors used for AOPs, titanium dioxide (TiO_2) stands out from others because of its high photochemical stability, low toxicity and cost to practical applications and scalability. TiO_2 also presents more availability to generate reactive oxygen species (ROS) which are responsible to degrade the organic pollutants. As a consequence, TiO_2 is the most used photocatalyst for various contaminants being the most effective and benign for the environment.

The photocatalytic properties of TiO_2 are strongly influenced by several factors, such as; particle size, crystal phase, morphology, crystalline defects, irradiation light, pH of suspension, specific surface area and preparation method of the photocatalytic material.[5,6] Jang and co-workers[7] mentioned that, among these factors, the most important are crystal structure and particle size, and therefore surface area related to the volume of the particle.

There are a large number of reports in the literature regarding TiO_2 with different sizes, crystalline phase morphologies and surface area, specifically applied to water remediation.[8-10] However, the understanding of how these parameters affect photocatalytic properties and the order of influence on the performance of these properties is an important problem or bottleneck that prevents its practical application. Up to date, to the best of our

knowledge, it has not been possible to control several of these parameters simultaneously, and their impact on the degradation of organic pollutants.

In terms of morphology, several geometries were recently reported, such as for example spherical titania nanostructures or hierarchical nanofibers, nanowires and hollow-fibers.[11-13] In this sense, Wang et al. recently reported that TiO_2 nanowires synthesized by the hydrothermal method presented an increased performance for hydrogen production.[14] Regarding their crystalline phases, anatase has received the most attention due to its high catalytic activity and electron mobility compared to the rutile and brookite phases,[15,16] because it exhibits more defects than other phases and therefore it has more sites available for oxygen to generate ROS. On the other hand, various works have shown a higher photocatalytic performance when using a mixture of crystalline phases containing anatase and rutile, especially TiO_2 Degussa P25 (commonly used as commercial photocatalyst) than a pure phase.[17] This improvement can be attributed to a synergic effect that is generated in the junction of the phases generating a decrease of the recombination of the hole-electron pairs.[18]

Several other works can be found related to TiO_2 and persistent water pollutants using different morphologies, crystal phases and sizes such as; nanostructures, nanocomposites, or hybrid photocatalysts, among others.[19-22] Lei and co-workers[23] reported a mixture of TiO_2 phases, improving the photocatalytic activity to degrade an organic dye in comparison to pure crystalline phases of TiO_2. Likewise, Juncheng et al.[24] described the synthesis of uniform rhombic nanoplates with a high photocatalytic performance by controlling the morphology of these nanostructures through a novel solvothermal method. They attributed the enhanced photocatalytic properties of TiO_2 nanoplates to degrade

methylene orange (99.6%) at 24h to the exposed {010} facets and the high surface areas. In this regard, Li et al.[25] have reported improvements in photocatalytic performance of TiO_2 to degrade methylene blue (MB) using CuS nanoflowers on a rutile surface. Additionally, Stoyanova and co-workers[26] demonstrated that a decrease in particle size is linked to a better photocatalytic performance. Atitar et al. also studied the effect of the calcination temperature and phase transformation on photocatalytic performance.[27]

One of the key parameters to control the shape and morphology of the catalyst is the synthetic method employed. Several methods to prepare TiO_2 nanostructures in solution using different conditions, such as the effect stabilizer, reductant and synthesis temperature have been developed.[28] The major problem of using solution phase methods is that the incorporation of metal-oxide nanoparticles into solid devices is not straightforward, since solid-state isolation of nanoparticles causes particle agglomeration. The most widely used method for preparing powdered TiO_2 is the sol-gel solution method, because a controllable morphology, high purity and homogeneity are achieved.[29] However, it has a number of disadvantages preventing the control of the factors that contribute to increasing the photo-response. For example, a difficult control of particle growth (implying a reduction of the surface area), resulting also in more aggregate structures. In addition, the crystallinity of the powder could also decrease, even becoming amorphous (influencing the sites available for O_2).[30] The incorporation of metal-oxide nanoparticles generated directly from a solid-state approach will be of great applicability. From our best knowledge, solid-state methods have scarcely reported to preparing TiO_2 nanoparticles.[31,32] For example, a solid-state metathesis reaction of $TiCl_3$ and Na_2O_2 in presence of NaCl to give variable mixtures of anatase and rutile[33] has been achieved. The reported photocatalytic activity of the obtained product

containing some anatase phase was comparable to a commercial TiO_2 standard. Other method consists of the anhydrous reaction of $TiOSO_4$ with Na_2CO_3 in presence of NaCl.[34] The average particle size, morphology and phase were strongly affected by the temperature of the post-milling heat treatment. The methods mentioned above, whether in solution or in the solid phase, have disadvantages with respect to the control of key factors in photocatalytic performance.

Park and co-workers have reported an interesting method to obtain TiO_2 fused particles in nanopowder, by means of a solid titanium precursor (TiH_2) in a thermal plasma reactor, being able to control the size of the nanostructures remarkably (20- 50nm) when compared to other processes, implying improved photocatalytic performance (95% of RhB degradation in 5h). Additionally, the particles obtained are resistant to heat treatment, both phases (anatase and rutile) being maintained in a range of 400-800 °C.[34] Yang et al [35] described an interesting synthetic route to get TiO_2 mesoporous single crystals with various morphologies in a controllable way by hydrothermal method using a silica template. They pointed out the morphology, size, and phase of the TiO_2 structures can be easily tuned by experimental conditions.

The most of solid state methods to synthetize TiO_2 have some disadvantages since their preparation involves the use of sophisticated and expensive instruments, and the chemistry involved in their generation processes is limited. Thus, most of them usually afford mixtures of anatase and rutile phase. [36-38]

As a first result, we describe for the first time in this work a solid-state phase control, morphology and size of TiO_2 through the nature of the macromolecular complex precursor used. During the formation of TiO_2 nanoparticles, the Chitosan and Poly(styrene-

co-4-vinylpyridine) polymers act as solid-state templates producing areas after carbonization, where the TiO_2 will grow. It seems that the location of metal centers through the polymeric chain (i.e. the distance between the metal centers) strongly influence the morphology and particle size of the photocatalyst. Although Chitosan[39-43] and Poly(styrene-co-4-vinylpyridine)[44-46] stabilize metallic nanoparticles in solution, there are no reports of the behavior of solid-state template of these polymers. In this work, a versatile and novel method is reported to control morphology, size and crystalline phase, which can modulate the photocatalytic properties and potentially their practical application, through a solid state route. Finally, the very efficient photocatalytic degradation of methylene blue (MB) on different polymorphic forms of nanostructured TiO_2 is demonstrated.

2. EXPERIMENTAL SECTION

2.1 Preparation of precursors

Chitosan, Poly(styrene-co-4-vinylpyridine), Cp_2TiCl_2, $TiOSO_4$, $TiO(acac)_2$ were purchased from Sigma-Aldrich and used as received.

Synthesis of (Chitosan)·(Cp_2TiCl_2) 1:1; precursor (I)

Stoichiometric amounts of chitosan (0.703 g, 4.01 mmol) and Cp_2TiCl_2 (1.000 g, 4.01 mmol) were stirred in a Schlenk flask for 2 weeks at room temperature (RT) in dichloromethane (60 mL). The supernatant solvent was extracted with a syringe by decantation and then dried under low pressure to finally obtain a red-orange solid.

Synthesis of (PS-co-4-PVP)·(Cp_2TiCl_2) 1:1; precursor (II)

Stoichiometric amounts of PS-co-4.PVP (0.425 g, 4.01 mmol) and Cp_2TiCl_2 (1.000 g, 4.01 mmol) were stirred in a Schlenk flask for 2 weeks at room temperature (RT) in

dichloromethane (60 ml). The supernatant solvent was extracted with a syringe by decantation and then dried low pressure. An orange solid was finally obtained.

Synthesis of (Chitosan)·($TiOSO_4$) 1:1; precursor (III)

Stoichiometric amounts of chitosan (1.094 g, 6.25 mmol) and $TiOSO_4$ (1.000 g, 6.25 mmol) were stirred in a Schlenk flask for 2 weeks at RT in dichloromethane (60 mL). The supernatant solvent was extracted with a syringe by decantation and then dried under reduced pressure. Finally, a white solid was obtained.

Synthesis of (PS-co-4-PVP)·($TiOSO_4$) 1:1; precursor (IV)

Stoichiometric amounts of PS-co-4-PVP (0.661 g, 6.25 mmol) and $TiOSO_4$ (1.000 g, 6.25 mmol) were stirred in a Schlenk flask for 2 weeks at RT in dichloromethane (60 mL). The supernatant solvent was extracted with a syringe by decantation and then dried under reduced pressure. A white solid was finally obtained.

Synthesis of (Chitosan)·$TiO(acac)_2$ 1:1; precursor (V)

Stoichiometric amounts of chitosan (0.668 g, 2.55 mmol) and $TiO(acac)_2$ (1.000 g, 2.55 mmol) were stirred in a Schlenk flask for 2 weeks at RT in dichloromethane (60 mL). The supernatant solvent was extracted with a syringe by decantation and then dried under reduced pressure. A yellow solid was finally obtained.

Synthesis of (PS-co-4-PVP)·$TiO(acac)_2$ 1:1; precursor (VI)

Stoichiometric amounts of PS-co-4-PVP (0.404 g, 1.54 mmol) and $TiO(acac)_2$ (1.000g, 1.54 mmol) were stirred in a Schlenk flask for 2 weeks at RT in dichloromethane (60 mL). The supernatant solvent was extracted with a syringe by decantation and then dried under reduced pressure. Finally, a pale yellow solid was obtained.

2.2 Pyrolysis of macromolecular complexes

The nanostructured TiO2 was obtained as follows; the macromolecular complexes were pyrolized in a porcelain crucible into an oven, model LEF-105S-1, LabTech brand in air at 500 °C, 600 °C, 700 °C and 800 °C for 4 h, with a heating rate of 10 °C/ min .

2.3 Structural and microstructural characterization

Powder X-Ray Diffraction (PXRD) were carried out at RT using a Siemens D-5000 diffractometer. PXRD data was collected using Cu- Kα radiation (40 kV and 30 mA) and a graphite monochromator (λ = 1.540598Å). The TiO_2 anatase phase was indexed as a tetragonal lattice (space group $I4_1$) with the following parameters: a = 3.7845 Å, c = 9.5143 Å, while the tetragonal TiO_2 rutile phase (space group $P4_2$) lattice parameters were a = 4.5940 Å and c = 2.9586 Å.

Scanning Electron Microscopy Field Emission (FE-SEM) micrographs were performed using a Merlin FE-SEM microscope (Carl Zeiss).

High-Resolution Transmission Electron Microscopy (HR-TEM) and *Selection Area Electron Diffraction* (SAED) was performed using a JEOL 2000FX TEM microscope at 200 kV to characterize the average particle size, distribution and elemental and crystal composition. The average particle size was calculated using the DigitalMicrograph software. Reflectance diffuse were measured by *UV-Vis absorption spectroscopy* performed on a Shimadzu UV-2600 IRS plus spectrophotometer.

2.3 Photodiscoloration Experiments

MB was used as a model compound to test the morphology, crystal phase and particle sizes-dependent on photocatalytic properties. The TiO_2 nanostructure activity was evaluated by measuring the decoloration rate of MB at 655 nm under UV-Vis illumination using a xenon lamp (150W) positioned 20 cm away from the photoreactor in a range 330-

680 nm at room temperature, to avoid the self-degradation and thermal catalytic effects of cationic dye MB. The short-wavelength components ($\lambda < 340$ nm) of the light were cut-off using a $CuSO_4$ optical filter (0.1 mol L^{-1}). 26 mg of the photocatalyst and 25 mL of MB aqueous solution (1 x 10^{-5} mol L^{-1}) were placed in a photoreactor vessel with continuous magnetic stirring. The suspension was stirred in the darkness for 60 min to establish an adsorption/desorption equilibrium, after which the photocatalytic decoloration of MB was initiated. Samples were withdrawn from the reactor at certain time intervals (5 min), and centrifuged to remove the particles.

3. RESULTS AND DISCUSSION

3.1 Characterization of the Macromolecular precursors

The synthesis of the macromolecular complexes was carried out by direct reaction of the respective polymer with the Ti compound in CH_2Cl_2. In this media, the polymers are partially soluble and the Ti compounds are: Cp_2TiCl_2 – soluble, $TiOSO_4$ – insoluble, and $TiO(acac)_2$ – partially soluble. Subsequently, the suspension was slowly transforming into an insoluble solid that can be easily separated from the solution by decantation. The solid acquires the colour of their respective Ti compounds, ie. Cp_2TiCl_2 red-orange, $TiOSO_4$ white and $TiO(acac)_2$ yellow (see Supp. Info. Fig. S1). The macromolecular complexes were characterised by IR spectroscopy, ^{13}C MAS NMR spectroscopy and TG/DTA analysis.

The presence of both polymers in the macromolecular complexes were confirmed by solid state ^{13}C NMR analysis. As shown in Fig. S2 (see Supp. Info), and as also found in other reports,[47,48] typical bands of Chitosan and PS-co-4-PVP were observed.[49-51]

As shown in Figure S3, additional information of the coordination of Ti compounds to chitosan and PS-co-4-PVP arises from the IR spectra of the macromolecular complexes. Coordination was confirmed by the shifting of a broad band of ν(OH)+ ν(NH) observed in a range of 3422-3338 cm^{-1} for (I), (III) and (V) complexes, compared to the same band observed for free chitosan at 3436 cm^{-1}. Furthermore, the NH_2 bending vibration is shifted to lower energy frequencies upon coordination. For macromolecular complexes with PS-co-4-PVP (II), (IV) and (VI), a shift of the characteristic vibration of νPy is observed in the range of 1576-1632 cm^{-1}.

TG/DTA analysis for the macromolecular complexes exhibits loss weigh patterns that are different to that of free chitosan (see Fig. S4), evidencing the coordination of the Ti moieties to the polymeric chain. However, the final weigh residue was in general slightly lower than the calculated values for TiO_2, probably due to a lesser coordination degree than 100%.

3.2 Pyrolytic products characterization

The pyrolysis (p) of different macromolecular complexes (I)-(VI) was studied at temperatures ranging from 500 to 800 ºC (TiO_2(precursor)p-temperature). A summary of the different TiO_2 obtained phases, sizes and morphologies at each of the studied temperatures can be found in Table 1.

Figure S5 shows the PXRD patterns for the pyrolytic product at 800 °C from TiO_2(I)p to TiO_2(VI)p. PXRD patterns for other pyrolytic products at different temperatures can be found in Fig. S5 (supplementary information). It is well stablished that rutile is the stable phase, while both anatase and brookite are metastable. The irreversible anatase to rutile transformation has been studied widely at different temperatures. However, the

factors affecting this phenomenon, such as crystal phase transformation, are not fully understood.[52] In this sense, as shown in Table 1, unexpected results were observed for the TiO_2(III)p, as there is no phase transformation from anatase to rutile in all the studied temperature range (from 500 °C to 800 °C). This remarkable result could be attributed to a kinetic effect due to the metastable nature of anatase.[53] Another interesting observation is the partial transformation of anatase to rutile for the products TiO_2(II)p, TiO_2(IV)p and TiO_2(V)p, which could be attributed to the same kinetic factor involved in this phase process, as shown in Table S1.[54]

The expected complete anatase to rutile transformation occurs for the pyrolysis of the precursors (I) and (VI). Additionally, it can be noted that for lower calcination temperatures, all the obtained products TiO_2(I)p-TiO_2(VI)p correspond to anatase. A small effect of the phase with the nature of the Ti salt linked to the polymeric chain of the polymer precursor –at fixed temperature- was also observed. For instance, at 800 °C the only precursor containing the $TiOSO_4$ salts linked to chitosan gives the anatase phase, while that both the precursor (I) and (VI) induces the rutile phase transformation.

The influence of the precursor on the structure´s morphology was studied by SEM, which is summarized in Table 1. Different polymorphic forms were found such as; microfibers, dense plates and irregular structures, as shown in Figure 1. These morphologies depend on the nature of the precursor used to synthesize the macromolecular complex. Interestingly, for TiO_2(III)p and TiO_2(IV)p the presence of $TiOSO_4$ linked to the polymeric chain induce the formation of microfibers formed by fused nanoparticles on the surface, leading to large surface areas (see Figure 1), which are in concordance to literature mentioned above. This seems to be independent of the polymer and pyrolysis temperature.

Additionally, for the pyrolytic products TiO_2(V)p and TiO_2(VI)p, the $TiO(acac)_2$ salt strongly influences the obtaining of irregularly shaped structures and 3D mesh-like regions, which are typical for metal oxide nanostructures obtained by pyrolytic methods. These interesting results reveal an opportunity in the rational design and controlled synthesis of TiO_2 structures with different morphologies by polymeric precursors.

TEM analysis of the different samples is shown in Table 1. In all cases, there is a strong size dependence on the nature of the Ti precursor and the polymer. As expected, particle sizes increase when increasing the calcination temperature, as also reported in previous works.[35] However, it is very remarkable that, for the pyrolytic product TiO_2-A-(III)p-800, a bimodal distribution of nanoparticles was obtained (Figure 2c). As shown in Figure 2, despite of the high calcination temperature, the smallest particle sizes (6.9±0.2 nm), in form of anatase, were found for these conditions and in four analysed temperatures.

TEM analysis demonstrates that the microstructure observed for all cases are fused TiO_2 nanoparticles of different crystal phases, which are in agreement with previous works.[55] Some insight about the formation mechanism of the nanostructured materials from the precursor Chitosan●MXn and PS-co-4-PVP●MXn could be proposed using the mechanism of formation of nanostructured metallic materials from the precursor $\{NP(OC_8H_{12})_2(OC_6H_4PPh_2\text{-}Mn(CO)_2(\eta^5\text{-}C_5H_4Me)_2\}$.[56]

The first step on heating involves the formation of a 3D network to produce a thermally stable matrix.[57] This step is crucial as it offset the sublimation. In our system, the first heating step could involve a cross linking of the Chitosan and PS-co-4-PVP polymers to give a 3D matrix, containing O-Ti-O and H_2N-Ti-NH_2 links (for the Chitosan polymer) and (pyridine)N-Ti-N(pyridine) bonds for the PS-co-4-PVP polymer. A schematic

representation of this process is provided in Figure 3. We believe that the following steps involve the starting of the organic carbonization, producing holes where the nanoparticles begin to nucleate. According to TG/DTA analysis, this occurs at ~ 128-401 °C for the Chitosan and 184-404 °C for PS-co-4-PVP polymer matrices. In this intermediate stage, a layered graphitic carbon host can act as a template, where the nanoparticles grow.[57] After complete combustion this template disappears, but always remains carbon residues, which appears as an ultrathin carbon shell around the nanoparticles, which were evidenced by TEM analysis. It is clear that the precursor polymers play a key role during nucleation process of the TiO_2 into the anatase or rutile phase. However, this step is not completely elucidated. It is very remarkable the formation of the anatase phase for TiO_2(III)p in all the studied conditions, being this very promissory photocatalyst material for remediation processes, due to their phase and morphology.

As shown in Table 1, and the absorption edge extrapolation (Figure S7) confirms band gap energies higher than bulk values, which are in concordance to quantum confinement effect of smaller TiO2 nanostructures. On the other hand, the tendencies regarding to crystal phase are in agreement to the previously reported band gap energies. However, there is no direct correlation of the morphology with respect to Eg. We can infer that the morphologies are related to the particle sizes that make up the structure. For example, microfibers are composed of small fused particles which are exposed to the surface, so they are associated with the size of the system. In this regard, the dense plates & irregular structures show lower band gap values, which we can attribute to their greater particles sizes. We can see that energy gaps must be considered in the irradiation to

quantify the photocatalyst performance, all of which are in the emission range of the solar spectrum (330 nm-680 nm equivalent to 3.75 eV-1.82 eV).

This novel reported method permits a control of the phase by selecting the appropriate Ti compound and the precursor polymer, ie. TiO_2(III)p precursor affords the formation of the anatase phase, and also the morphology and particle size can be tuned by the appropriated selection of these parameters (see Table 1). This method presents a clear advantage over another solid-state and solution methods, as an effective control of key parameters can be achieved governing the photocatalytic response for practical applications. Another additional advantage is that, from our method, TiO_2 nanopowders are directly obtained, which can be used directly for their incorporation in a solid device avoiding an agglomeration process.

3.4 Photocatalytic behavior of TiO_2 nanostructures

The photocatalytic performance of a persistent water pollutant for all TiO_2 systems was investigated by quantifying the discoloration rate and pseudo-first-order rate constants of MB with UV-vis irradiation (330-670nm) and the better system are shown in Figure 4. The UV−vis absorption spectra and the normalized concentration changing of MB as a function of irradiation time for all TiO_2 nanostructures obtained by (I)p-(VI)p precursors at different temperatures can be found in Figures S8 and S9, respectively. The kinetic analysis (Figure S10) is also summarized in Table 2. Without photocatalyst, we observed that the MB dye has a slight decoloration (~ 7%), indicating that the degradation of the organic pollutant by UV-vis light is scarce. A highest MB photodegradation (86.5%, see Figure 4a and 4b) at pH 6.5 and 25 min of irradiation time for TiO_2 in anatase phase obtained from (III)p at 800°C have been achieved. It is very remarkable that highest extent degradation

was obtained after few minutes for the anatase microfibers formed by TiO_2 fused nanoparticles (TiO_2-A-(III)p-800), compared with commercial TiO_2 (Degussa P25) which only degraded 75.5% of MB at the same experimental conditions.

As shown in Figure 5, we investigated the influence of morphology, size and crystal phase of our photocatalytic materials to discoloration of MB to establish a correlation of these key factors in the photocatalytic behavior. These results demonstrate that the structures with better performances are those of microfiber morphology and then irregular structures. The morphologies that showed smaller photocatalytic yields are those of dense plates and dense & irregular, which are in concordance to their optical properties obtained by DRS and smooth and greater surfaces observed by SEM, avoiding the high photocatalytic response. We attribute these results to microfibers´ structures, due are composed of fused small particles exposed to the surface, which leads to greater chemical reactivity to interact to MB and an anatase phase, in agreement to the optical properties.[54] If we analyse our systems that have the same morphology and similar sizes, we can find a correlation of how much the crystalline phase influences the photocatalytic performance (see Figure 5). The results allow showing the influence exerted by the crystal phase on the photocatalytic performance, being the following: mixture > anatase > rutile. For example, if we compare TiO_2-A-(I)p-500 and TiO_2-M-(I)p-600, both have the same morphology (granular) and similar sizes (11 and 12 nm) but the crystal phase is different (anatase and mixture, respectively). TiO_2-M-(I)p-600 shows a 20.4% of decolouration rate comparatively with 10.9% for TiO_2-A-(I)p-500, evidencing that mixture is better than anatase. These results are in concordance with Bacsa and co-workers.[58] They have attributed this behaviour to that a mixture of phases has a greater charge separation than a

pure phase between the interface, because the electrons are strongly retained in the electronic bands of the rutile, decreasing the charge recombination of the electron-hole pairs, which leads to an increase in their photoresponse.

As shown in Figure 5, if we compare the sizes of the systems when the phases and morphologies are the same, it can be observed that the behavior of the photocatalytic activities increases as the size decreases. These results are in agreement with those described in the literature, which report that decreasing the sizes increases the chemical reactivity and therefore the photocatalytic performance is greater.[59]

It is very interesting to note in Table 2, that the TiO_2(III)p samples for all temperatures show the same phase and morphology, therefore the photocatalytic properties were the expected according to their particles sizes as mentioned above. Therefore, from these remarkable results, the present approach provides the first evidence of a highly efficient photocatalytic decoloration using pristine TiO_2 systems in a short time. Additionally, according to our results, we can estimate the order of factors that control the photocatalytic properties, using a statistic study by Principal Component Analysis (PCA), as shown in Figure S11. The PCA has evidenced that the main components that impact on the photoresponse are size and crystal phase, since they explain 85% of the variance. According to the statistical analysis and the structural and band gap energies we can attribute the following order: Particle size > crystal phase > morphology (in close relation to the features of the surfaces)

The photodegradation process can be further quantitatively interpreted through fitting to the Pseudo-first order reaction model (assuming that the photocatalyst concentration is constant), in which apparent constant (k) of MB photodegradation can be

determined according to the following expression: $\ln(C/C_o) = -kt$, where C_o and C are the concentrations of MB at initial and a certain irradiation time, and k is the slope of the fitting line. This apparent rate constant is a very good parameter to compare the photoresponse of the studied systems. In this regard, the pseudo-first-order rate constants reported in Table 2 are in good agreement and have the same trends to the discoloration rate results and reveal that the best photocatalyst TiO_2-A-(III)p-800 provides 118.8 times higher degradation rate than TiO_2-M-(I)p-700. The normalized results summarized in Table 2 still show the same trend in performance and confirm that the TiO_2-A-(III)p-800 has the most efficient photodegradation activity. In addition, the catalytic activities and trend in performance measured herein are consistent with those measured in previous reports highlighting the quality of the TiO_2 nanostructures and their different phases.[15,16]

To analyze our results in a comprehensive way, and in the same context against other state-of-the-art TiO_2 materials, we have compared them with other efficient catalysts in the literature. The comparison was performed with pure TiO_2 phases, using MB and other persistent organic pollutants within different crystal phases, morphologies, sizes and their correlation with photocatalytic performance to degrade water pollutants. This analysis (see Table 3) was carried out considering the main conditions that dictate the photocatalytic activity, which was described in the introduction section. In spite of the great number of available works in the literature related to TiO_2, the three aforementioned factors have not been controlled simultaneously, and also their order of importance to control the photochemical reactions.

From the comparative analysis of state-of-the-art materials with the ones here reported, our remarkable results arise on very high efficient photodiscoloration of MB in a

short time, and also in a better comprehension and control of the main factors that government the photocatalytic response of TiO_2. Our results suggest that, in order to achieve very efficient photocatalytic properties, we must use a system that has fibers formed of fused nanoparticles, anatase phase and small sizes less than 10 nm. In order to outperform the activity of Degussa P25, up to now, the addition of another phase was necessary to enhance efficiency. From our knowledge, the present results (TiO_2-A-(III)p-800) showed the most efficient photocatalyst reported in the literature, in a short time, using pure TiO_2 without the addition of any other phase or dopant. In this regard, to take advantage of the TiO_2-A-(III)p-800 abilities, we have analyzed the pH effect on the rate of the photocatalytic process, because is the major factor influencing the discoloration rate.[71] Fig S12 shows the discoloration percentage as a function of pH for TiO_2-A-(III)p-800 and commercial TiO_2. An improvement of MB discoloration rate in alkaline medium was observed for both compounds. The highest photodegradation was observed in alkaline medium to pH 9 for TiO_2-A-(III)p-800 and commercial TiO_2 P25, reaching 98% and 77% respectively. According to the literature, these improvement is expected because in an alkaline medium the adsorption of MB is considerably enhanced.

Finally, another important aspect to be considered for the practical application of the photocatalyst is its separation of the treated water for its reusability and scalability. These aspects were investigated by the photocatalytic efficiency of TiO_2-A-(III)p-800 for several cycles. The photocatalyst was removed by filtration from the dispersion after degradation of MB, washed with water and ethanol and dried at RT. Subsequently, it was reused to photochemically degrade a fresh MB solution. The results of photocatalyst reusability are shown in Figure 4d. The four cycles carried out for the photodegradation of

MB showed that the efficiency of TiO_2-A-(III)p-800 remains high, the percentage of photodegradation (~86%, pH 6.5) is practically unchanged compared to the first use.

4. SUMMARY AND CONCLUSIONS

A simple solid state synthetic pathway using macromolecular complexes has been developed to prepare TiO_2 nanostructures in different morphologies, crystalline phases and sizes. The proposed mechanism suggests a cross linking of the Chitosan and PS-co-4-PVP polymers to give a 3D matrix when it heated. Subsequently, the following steps involve the formation of holes that act as nucleation centers of the nanostructures. Therefore, it can be concluded that the precursor polymers and the nature of the Ti precursor play a fundamental role in the mechanism of formation of fused TiO_2 nanoparticles. The obtained TiO_2 nanostructures present an efficient photocatalytic decoloration a short time and the factors controlling their photocatalytic properties are the size and then crystal phase and subsequently the morphology, in close relation to the features of the surface. This three aforementioned factors have not been controlled simultaneously, and also their order of importance to control the photochemical reactions. The best photocatalyst was able to degrade the MB (discoloration rate) by 98% in only 25 min measured at 655 nm, in alkaline medium. These important results allow the rational design of a photocatalyst to control the characteristics of the material and water pollutants to achieve very efficient performances concerning the treatment and removal of recalcitrant. In this sense, the improvement of chemical reactivity towards other family substrates, such as phenols, anionic and azo dyes

which are hazardous pollutants or chemical transformations could improve the performance of these catalysts.

ASSOCIATED CONTENT

Supporting Information available: ^{13}C MAS NMR and IR spectra, TG/DTA curves of all macromolecular complexes and pure polymers. PXRD, crystal phase quantification and degradation curves of MB for TiO_2 systems are available on the ACS Publications website

AUTHOR INFORMATION

ORCID

Patricio Allende: 0000-0003-0299-6246

M. Angel Laguna-Bercero: 0000-0002- 7819-8956

Lorena Barrientos: 0000-0002-9641-6507

Maria Luisa Valenzuela: 0000-0002- 5759-2110

Carlos Díaz: 0000-0002- 4535-4115

ACKNOWLEDGEMENTS

The authors acknowledge Fondecyt Projects 1120179, 1160241 and Faculty of Chemistry grant UC-3913-529-81 for financial support. This research has also received funding from Consejo Superior de Investigaciones Científicas, Spain under grant I-COOP LIGHT 2015CD0013. The use of Servicio General de Apoyo a las Investigación (SAI, University of Zaragoza) is also acknowledged.

REFERENCES

(1) Wang C.; Li J.; Liang X.; Zhang Y. and Guo G., Photocatalytic Organic Pollutants Degradation in Metal–Organic Frameworks, *Energy Environ. Sci.* **2014**, *7*, 2831–2867.

(2) Wang D.; Silbaugh T.; Pfeffer R. and Lin Y. Removal of Emulsified Oil from Water by Inverse Fluidization of Hydrophobic Aerogels, *Powder Technol.* **2010**, *203*, 298–309.

(3) Lin D.; Zhao Q.; Hu L. and Xing B. Synthesis and Characterization of Cubic Mesoporous Bridged Polysilsesquioxane for Removing Organic Pollutants from Water, *Chemosphere*, **2014**, *103*, 188–196.

(4) Wang G.; Yang L.; Wu F.; Deng N. Carboxymethyl-β-Cyclodextrin Enhanced TiO_2 Removal of Acid Red R and Lead Ions in Suspended Solutions, *J Chem Technol Biotechnol,* **2014**, *89*, 297-304.

(5) Ichijo T.; Sato S. and Fujita M. Size-, Mass-, and Density-Controlled Preparation of TiO_2 Nanoparticles in a Spherical Coordination Template, *J. Am. Chem. Soc.*, **2013**, *135*, 6786–6789.

(6) Pagliaro M.; Palmisano G.; Ciriminna R.; Loddo V. Nanochemistry Aspects of Titania in Dye -Sensitized Solar Cells, *Energy Environ. Sci.*, **2009**, *2*, 838-844.

(7). Jang H.; Kim S.; Kim S. Effect of Particle Size and Phase Composition of Titanium Dioxide Nanoparticles on the Photocatalytic Properties. *J. Nanopart. Research*, **2007**, *3*, 141-147.

(8) Ge M.; Cao C.; Huang J.; Li S.; Chen Z.; Zhang K.; Al-Deyab S. S. and Lai Y. A Review of One-Dimensional TiO2 Nanostructured Materials for Environmental and Energy Applications. *J. Mater. Chem. A*, **2016**, *4*, 6772-6801.

(9) Alsawat M.; Altalhi T.; Shapter J. G. and Losic D. Influence of Dimensions, Inter-distance and Crystallinity of Titania Nanotubes (TNTs) on their Photocatalytic Activity. *Catal. Sci. Technol.*, **2014**, *4*, 2091-2098.

(10) Lai Y. K.; Sun L.; Chen Y. C.; Zhuang H. F.; Lin C. J. and Chin J. W. Effects of the Structure of TiO_2 Nanotube Array on Ti Substrate on its Photocatalytic Activity. *J. Electrochem. Soc.*, **2006**, *153*, D123-D127.

(11) Liu G.; Yu J. C.; Lu G. Q.; Cheng.M-H. Crystal Facet Engineering of Semiconductor Photocatalysts: Motivations, Advances and Unique Properties. *Chem. Commun.*, **2011**, *47*, 6763-6783.

(12) Kumar P. S.; Sundaramurthy J.; Sundarrraja S.; Babu V. J.; Singh G.; Allakhverdiev S.I.; Ramakrishna S. Hierarchical Electrospun Nanofibers for Energy Harvesting, Production and Environmental Remediation. *Energy Environ Sci.*, **2014**, *7*, 3192-3222.

(13) Chen D. and Caruso R.A. Recent Progress in the Synthesis of Spherical Titania Nanostructures and their Applications. *Adv Funct Mater.*, **2013**, *23*, 1356-1374.

(14) Bierman M.J. and Jin S. Potential Applications of Hierarchical Branching Nanowires in Solar Energy Conversion. *Energy Environ Sci.*, **2009**, *2*, 1050-1059.

(15) Wang G.; Wang H.; Ling Y.; Tang Y.; Yang X.; Fitzmorris R.C.; Wang C.; Zhang J.Z.; Li Y. Hydrogen-Treated TiO_2 Nanowire Arrays for Photoelectrochemical Water Splitting. *Nano Lett.*, **2011**, *11*, 3026-3033.

(16) Li R.; Weng Y.; Zhou X.; Wang X.; Chong Y. M.; Han H. and Li C. Achieving Overall Water Splitting Using Titanium Dioxide-based Photocatalysts of Different Phases. *Energy Environ. Sci.*, **2015**, *8*, 2377-2382.

(17) Ma Y.; Wang X.; Jia Y.; Chen X.; Han H. and Li C. Titanium Dioxide-Based Nanomaterials for Photocatalytic Fuel Generations. *Chem. Rev.*, **2014**, *114*, 9987-10043.

(18) Kho Y. K.; Iwase A.; Teoh W. Y.; Maedler L.; Kudo A.; Amal R. Photocatalytic H2 Evolution over TiO_2 Nanoparticles. The Synergistic Effect of Anatase and Rutile. *J. Phys. Chem. C* **2010**, *114*, 2821-2829.

(19) Ge M.; Cao C.; Huang J.; Li S.; Chen Z.; Zhang K.-Q.; Al-Deyab S. S. and Lai Y. A Review of One-dimensional TiO_2 Nanostructured Materials for Environmental and Energy Applications. *J. Mater. Chem. A*, **2016**, *4*, 6772-6801.

(20) Bennett J. A.; Wilson K. and Lee A. F. Catalytic Applications of Waste Derived Materials. *J. Mater. Chem. A,* **2016**, *4*, 3617-3637.

(21) Linsebigler A. L.; Lu G. and Yates Jr J. T. Photocatalysis on TiO_2 Surfaces: Principles, Mechanisms, and Selected Results. *Chem. Rev.*, **1995**, *95*, 735-758.

(22) Bakre P. V.; Volvoikar P. S.; Vernekar A. A. and Tilve S. G. Influence of Acid Chain Length on the Properties of TiO_2 Prepared by Sol-gel Method and LC-MS Studies of Methylene Blue Photodegradation. *J. Coll. Interf. Sci.*, **2016**, *474*, 58-67.

(23) Lei J.; Li H.; Zhang J. and Anpo M. Low-Dimensional and Nanostructured Materials and Devices Properties, Synthesis, Characterization, Modelling and Applications. *Springer International Publishing*, Switzerland, **2016**.

(24) Sun W.; Liu, H.; Hu, J. and Li, J. Controllable Synthesis and Morphology-dependent Photocatalytic Performance of Anatase TiO_2 Nanoplates. *RSC Adv.*, **2015**, *5*, 513-520.

(25) Lu, Y.Y.; Zhang, Y.Y.; Zhang, J.; Shi, Y.; Z.Li, Z.; Feng, Z.C. and Li., C. In Situ Loading of CuS Nanoflowers on Rutile TiO_2 Surface and their Improved Photocatalytic Performance. *Appl. Surf. Sci.*, **2016**, *370*, 312-319.

(26) Stoyanova A. M.; Ivanova, N.K.; Bachvarova-Nedelcheva, A. and Iordanova, R. Synthesis and Photocatalytic Performance of Fe (III), N co-doped TiO_2 Nanoparticles. *Bulgarian Chem. Coommun.*, **2015**, *47*, 330-335.

(27) Atitar, M. F.; Ismail, A. A.; Al-Sayari, S. A.; Bahnemann, D.; Afanasev, D. and Emeline, A. V. Mesoporous TiO_2 Nanocrystals as Efficient Photocatalysts: Impact of Calcination Temperature and Phase Transformation on Photocatalytic Performance. *Chem. Eng. J.*, **2015**, *264*, 417-424.

(28) Yang, J.; Mei, S.; Ferreira, J. M. F. Hydrothermal Synthesis of TiO_2 Nanopowders from Tetraalkylammonium Hydroxide Peptized Sols. *Mater. Sci. Eng. C*, **2001**, *C15*, 183-185.

(29) Wang Y.; He Y.; Lai Q.; Fan M.; Review of the Progress in Preparing Nano TiO_2: An Important Environmental Engineering Material. *J. Environm. Sci.*, **2014**, *26*, 2139-2177.

(30) Li, J.G.; Kamiyama, H.; Wang, X.H.; Moriyoshi, Y. and Ishigaki, T. TiO2 Nanopowders via Radio-frequency Thermal Plasma Oxidation of Organic Liquid Precursors: Synthesis and Characterization. *J. Eur. Ceram. Soc*. **2010**, *26*, 423-428.

(31) Dodd A.; McKinley A.; Tsuzuki T. and Saunders M. Optical and Photocatalytic Properties of Nanocrystalline TiO_2 Synthesised by Solid-state Chemical Reaction. *J. Phys. Chem. Solids*, **2007**, *68*, 2341-2348.

(32) Yang Z.; Choi D.; Kerisit S.; Rosso K.; Wang D.; Zhang J.; Graff G.; Liu J. Nanostructures and Lithium Electrochemical Reactivity of Lithium Titanites and Titanium Oxides: A review. J. *J. Power Sources.* **2009**, *192*, 588-598.

(33) Perera S.; Zelenski N. and Gillian G. Synthesis of Nanocrystalline TiO_2 and Reduced Titanium Oxides via Rapid and Exothermic Metathesis Reactions. *Chem. Mater.* **2006**, *18*, 2381-2388.

(34) Billik P.; Plesch G. Mechanochemical Synthesis of Anatase and Rutile Nanopowders from TiOSO4. *Materials Letters,* **2007**, *61*, 1183-1186.

(35) Zheng X.; Kuang Q.; Yan K.; Qiu Y.; Qiu J. and Yang S. Mesoporous TiO_2 Single Crystals: Facile Shape-, Size-, and Phase-Controlled Growth and Efficient Photocatalytic Performance. *ACS Appl. Mater. Interfaces* **2013**, *5*, 11249−11257

(36) Cao, F.; Xiong, J.; Wu, F.; Liu, Q.; Shi, Z.; Yu, Y.; Wang, X. and Li, L. Enhanced Photoelectrochemical Performance from Rationally Designed Anatase/Rutile TiO_2 Heterostructures. *Appl. Mater. Interfaces* **2016**, *8*, 12239–12245.

(37) Samal S.; Kim D.; Kim K.; Park D. Direct Synthesis of TiO_2 Nanoparticles by Using the Solid-state Precursor TiH2 Powder in a Thermal Plasma Reactor. *Chem. Eng. Res. Des*. **2012**, *90*, 1074-1081.

(38) Fattakova-Rohlfing D.; Zaleska A.; Bein T. Three-Dimensional Titanium Dioxide Nanomaterials. *Chem. Rev*. **2014**, *114*, 9487-9558.

(39) Kumar S. G.; Koteswara K. S. Polymorphic Phase Transition Among the Titania Crystal Structures Using a Solution-based Approach: from Precursor Chemistry to Nucleation Process. *Nanoscale* **2014**, *5*, 11574-11632.

(40) Huang H. and Yang X. Synthesis of Polysaccharide-stabilized Gold and Silver Nanoparticles: a Green Method. *Carbohydr. Res.*, **2004**, *339*, 2627-2631.

(41) Ding Y.; Xia X.H. and Zhang C. Synthesis of Metallic Nanoparticles Protected with N,N,N-trimethyl Chitosan Chloride via a Relatively Weak Affinity. *Nanotechnology* **2006**, *17*, 4156-4162.

(42) Okitsu K.; Mizukoshi Y.; Yamamoto T. A.; Maeda Y. and Nagata Y. Sonochemical Synthesis of Gold Nanoparticles on Chitosan. *Mater. Lett.* **2007**, *61*, 3429-3431.

(43) Yang K.H.; Liu Y.Ch.; Hsu T.Ch. and Tsai H.I. pH-insensitive Fabrication of Gold Nanoparticles with High Concentration by Ultrasound-assisted Electrochemical Process via Aid of Chitosan. *Mater. Res. Bull.,* **2010**, *45*, 63 68.

(44) Chang Y.Ch. and Chen D.H. Preparation and Adsorption Properties of Monodisperse Chitosan-bound Fe_3O_4 Magnetic Nanoparticles for Removal of Cu(II) Ions. *J. Coll. Interf. Sci.*, **2005**, *283*, 446-451.

(45) Wen F.; Zhang W.; Wei G.; Wang Y.; Zhang J.; Zhang M. and Shi L. Synthesis of Noble Metal Nanoparticles Embedded in the Shell Layer of Core−Shell Poly(styrene-co-4-vinylpyridine) Microspheres and Their Application in Catalysis. *Chem. Mater.* **2008**, *20*, 2144-2150.

(46) Klingelhöfer S.; Heitz W.; Greiner A.; Oestreich S.; Forster S. and Antoinietti M. Preparation of Palladium Colloids in Block Copolymer Micelles and Their Use for the Catalysis of the Heck Reaction. *J. Am. Chem. Soc*. **1997**, *119*, 10116-10120.

(47) Zheng P.; Jiang X.; Zhang X. and Shi L., Formation of Gold@Polymer Core−Shell Particles and Gold Particle Clusters on a Template of Thermoresponsive and pH-Responsive Coordination Triblock Copolymer. *Langmuir*, **2006**, *22*, 9393-9396.

(48) Johannesen, S.A.; Petersen, B.O.; Duus J.; Skrydstrup T. Studies Directed to Understanding the Structure of Chitosan−Metal Complexes: Investigations of Mono- and Disaccharide Models with Platinum(II) Group Metals. *Inorg. Chem.*, **2007**, *46*, 4326-4335.

(49) Kramareva N. V.; Stakheev A. Y.; Tkachenko O. P.; Klementiev K. V.; Grunert W.; Finashina E. D. and Kustov L. Heterogenized Palladium Chitosan Complexes as Potential Catalysts in Oxidation Reactions: Study of the Structure. *J. Mol. Catal. A: Chem.*, **2004**, *209*, 97-106.

(50) Saito H.; Tabeta R. and Ogawa K. High-Resolution Solid-state 13C NMR Study of Chitosan and Its Salts with Acids: Conformational Characterization of Polymorphs and Helical Structures as Viewed from the Conformation-Dependent ^{13}C Chemical Shifts. *Macromolecules*, **1987**, *20*, 2424-2430.

(51) Heux L.; Brugnerotto J.; Desbrieres J.; Versali M. F. and Rinaudo M. Solid State NMR for Determination of Degree of Acetylation of Chitin and Chitosan. *Biomacromolecules*, **2000**, *1*, 746-751.

(52) Chen, S.-C.; Kuo, S.-W. and Chang, F.-C. On Modulating the Self-Assembly Behaviors of Poly(styrene-b-4-vinylpyridine)/Octyl Gallate Blends in Solution State via Hydrogen Bonding from Different Common Solvents. *Langmuir*, **2011**, *27*, 10197-10205.

(53) Hanaor D. A.; Sorrell C. C. Review of the Anatase to Rutile Phase Transformation. *J Mater Sci,* **2011**, *46*, 855-874.

(54) Spurr R.; Myers H. Quantitative Analysis of Anatase-Rutile Mixtures with an X-Ray Diffractometer. *Anal Chem*. **1957**, 29, 760-762.

(55) Nalwa H.S. Encyclopedia of Nanoscience and Nanotechnology*, American Scientific Publishers Chapter 16*, New York, **2010**.

(56) Diaz C.; Barrientos L.; Carrillo D.; Valdebenito J.; Valenzuela M. L.; Allende P.; Geaneye H. and O'Dwyer C. Solvent-less Method for Efficient Photocatalytic α-Fe_2O_3 Nanoparticles Using Macromolecular Polymeric Precursors. *New J. Chem.,* **2016**, *40*, 6768-6776.

(57) Díaz C.; Valenzuela M.L.; Lavayen V.; O'Dwyer C. Layered Graphitic Carbon Host Formation during Liquid-free Solid State Growth of Metal Pyrophosphates. *Inorganic Chem*. **2012**, 51, 6228-6236.

(58) Díaz C.; Valenzuela M.L.; Zuñiga L. and O'Dwyer C. Organometallic Derivatives of Cyclotriphosphazene as Precursors of Nanostructured Metallic Materials: a New Solid State Method. *J. Inorg. Org. Polym. Mater*. **2009**, *19*, 507-520.

(59) Bacsa R.R. and Kiwi J. Effect of Rutile Phase on the Photocatalytic Properties of Nanocrystalline Titania During the Degradation of p-Coumaric Acid. *Appl. Catal. B*. **1998**, *16*, 19-29.

(60) Xu N.; Shi Z.; Fan Y.; Dong J.; Shi J. and Hu M.Z. Effects of Particle Size of TiO_2 on Photocatalytic Degradation of Methylene Blue in Aqueous Suspensions. *Ind. Eng. Chem. Res*., **1999**, *38*, 373-379.

(61) Sreekanth T.V.M.; Shim, J.-J and Lee, Y.R. Degradation of Organic Pollutants by Bio-Inspired Rectangular and Hexagonal Titanium Dioxide Nanostructures. *J.Photochem. Photobiol. B,* **2017**, *169*, 90-95.

(62) Topcu S.; Jodhani G.; Gouma P. I.; Optimized Nanostructured TiO_2 Photocatalysts. *Front. Mater*. **2016**, *3:35*, 1-9.

(63) Choudhury B.; Bayan, S.; Choudhury, A. and Chakraborty, P. Narrowing of Band Gap and Effective Charge Carrier Separation in Oxygen Deficient TiO_2 Nanotubes with Improved Visible Light Photocatalytic Activity. *J.Coll. Interf. Sci,* **2016**, *465*, 1-10.

(64) Chowdhury I.H.; Ghosh, S. and Naskar M.K. Aqueous-Based Synthesis of Mesoporous TiO_2 and Ag–TiO_2 Nanopowders for Efficient Photodegradation of Methylene Blue. *Ceram. Int.*, **2016,** *42*, 2488-2496.

(65) Liu S,; Yu J. and Jaroniec M. Tunable Photocatalytic Selectivity of Hollow TiO_2 Microspheres Composed of Anatase Polyhedra with Exposed {001} Facets. *J. Am. Chem. Soc*., **2010**, *132*, 11914-11916.

(66) Jang H.; Kim S. and Kim S. Effect of Particle Size and Phase Composition of Titanium Dioxide Nanoparticles on the Photocatalytic Properties. *J. Nanopart. Res.* **2001**, *3***,** 141-147.

(67) Wu Z.; Xue Y.; Zou Z.; Wang X.; Gao F. Single-Crystalline Titanium Dioxide Hollow Tetragonal Nanocones with Large Exposed (101) Facets for Excellent Photocatalysis. *J.Coll. Interf.Sci.*, **2017**, *490*, 420-429.

(68) Ryu J.; Kim W.; Kim J.; Ju J.; Kim J. Is Surface Fluorination of TiO_2 Effective for Water Purification? The Degradation vs. Mineralization of Phenolic Pollutants. *Catal. Today*, **2017**, *282*, 24-30.

(69) Xiong P.; Hu J.; Decomposition of Acetaminophen (Ace) Using TiO_2/UVA/LED System. *Catal. Today*, **2017**, *282*, 48-56.

(70) Samala S.; Kim D. W.; Kim K.S; Park D.W. Direct Synthesis of TiO_2 Nanoparticles by Using the Solid-State Precursor TiH_2 Powder in a Thermal Plasma Reactor. *Chem. Eng. Res. Des.* **2012**, *90*, 1074-1081.

(71) Tayade R.J.; Natarajan T.S.; Bajaj H.C. Photocatalytic Degradation of Methylene Blue Dye Using Ultraviolet Light Emitting Diodes Ind. Eng. Chem. Res. **2009**, *48*, 10262–10267.

Figures Caption

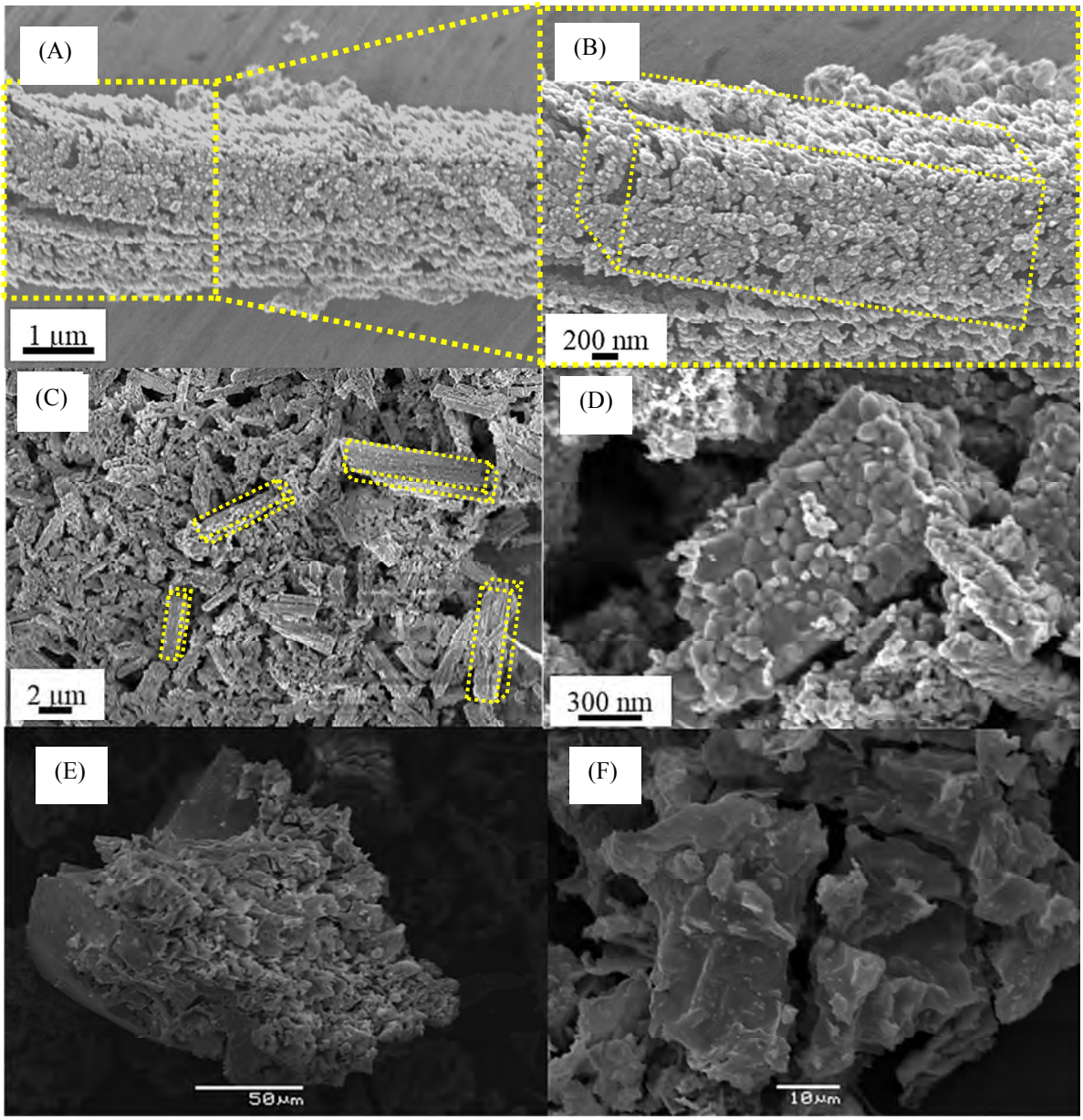

Figure 1. SEM images of (A) TiO_2-A-(III)p-800 showing a microfiber and (B) increased image of fused nanoparticles forming this structure, (C) and (D) showing the same microstructure for TiO_2-M-(IV)p-800, (E) TiO_2-M-(VI)p-500 evidencing irregular and (F) TiO_2-M-(I)p-600 dense plates morphologies.

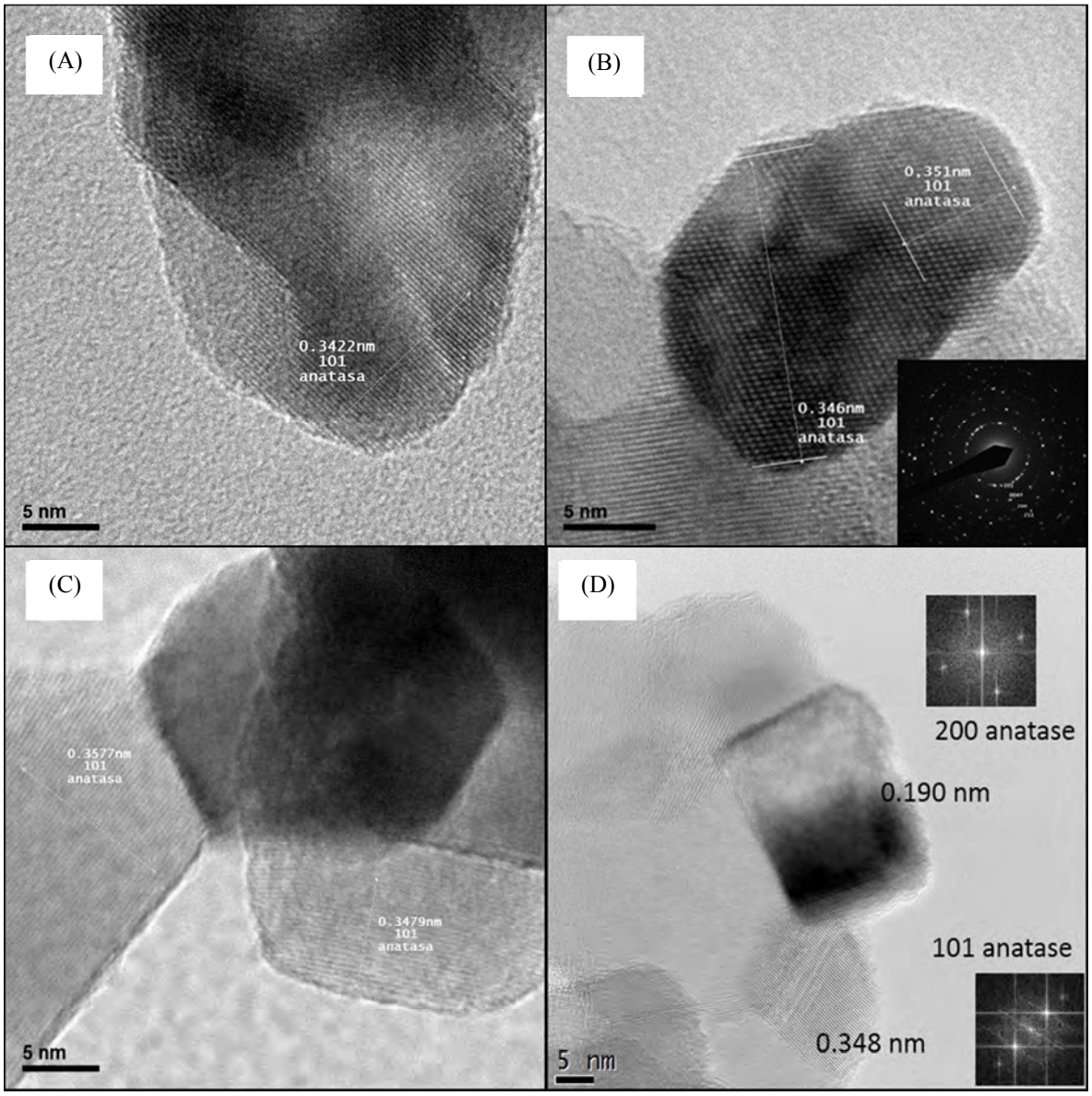

Figure 2. HRTEM images for TiO_2-A-(III)p microfibers composed of fused particles at different temperatures (A) 500 °C, (B) 600 °C, (C) 700°C and (D) 800 °C showing the crystal planes of anatase phase. The insets show the electron diffraction patterns of TEM images.

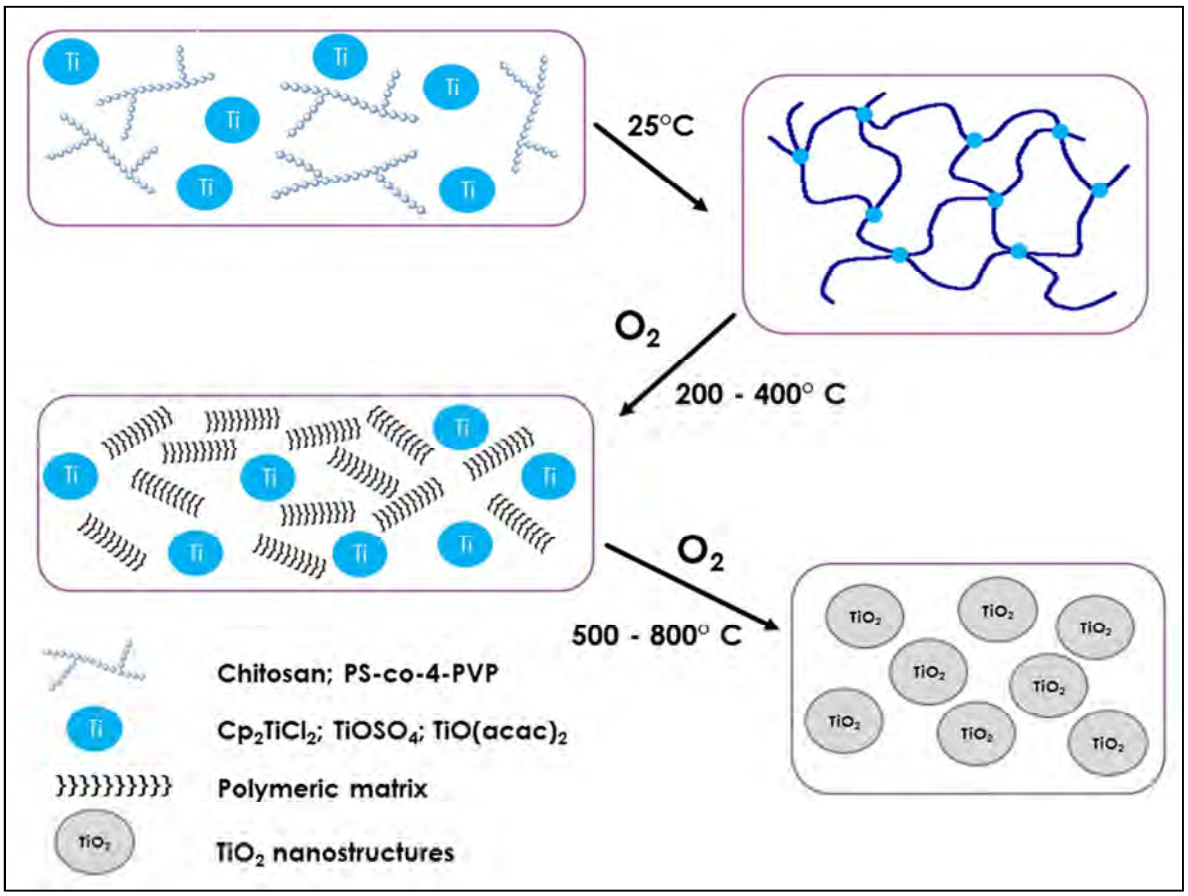

Figure 3. Schematic representation of the proposed mechanism in the formation of TiO_2 nanostructures. In the first step, at room temperature the formation of the 3D matrix occurs. Subsequently, the increase in temperature causes the decomposition of the polymer matrix and the formation of TiO_2 nanostructures.

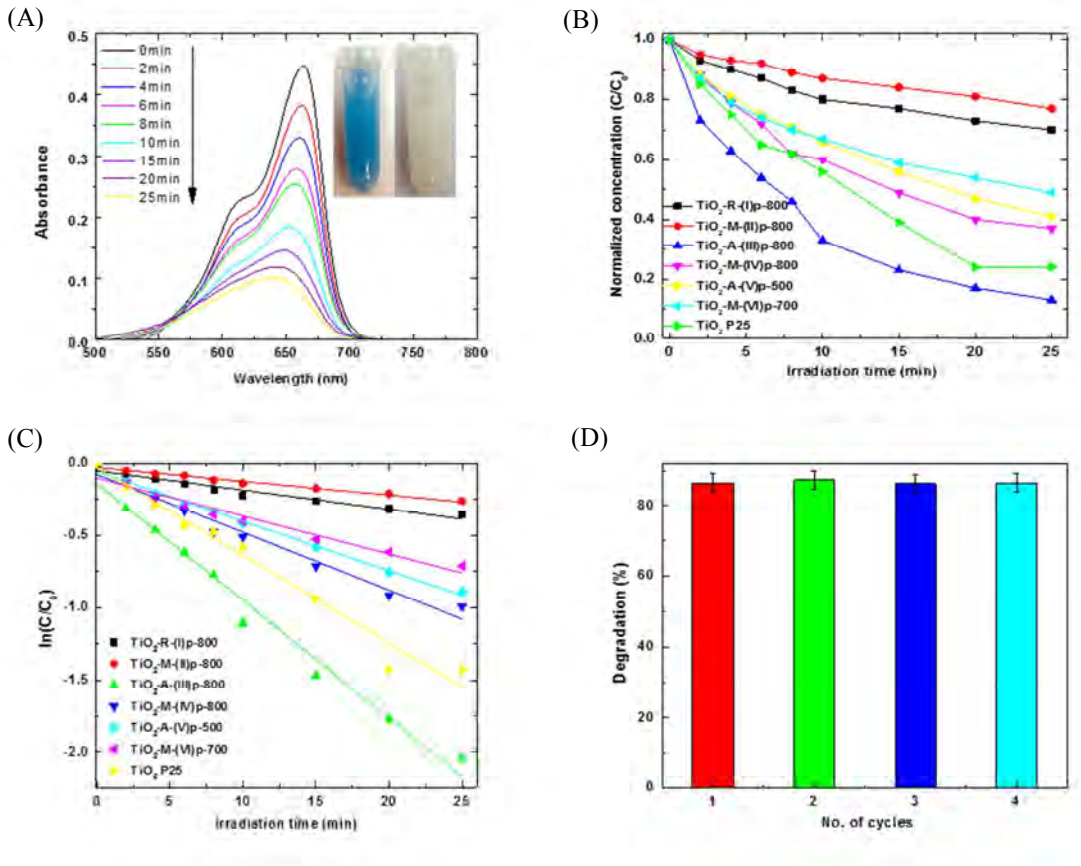

Figure 4. (A) Photodiscoloration curves of MB in presence of our best photocatalyst (TiO_2-A-(III)p-800). The inset shows changing of MB before and after photochemical reaction. (B) Normalized concentration of MB as function of irradiation time showing the best performances of TiO_2 nanostructures with different precursors and TiO_2 P25. (C) Pseudo-first order kinetic of photocatalytic reactions for this process. (D) Variation in the efficiency of the TiO_2-A-(III)p-800 for the degradation of MB with cycling. The exposure time in each cycle was 25 min.

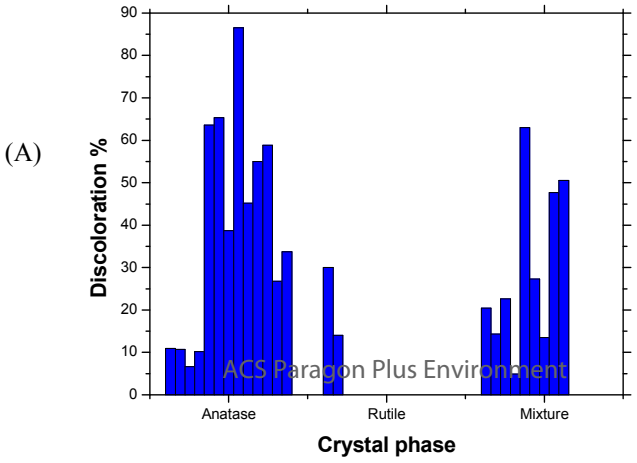

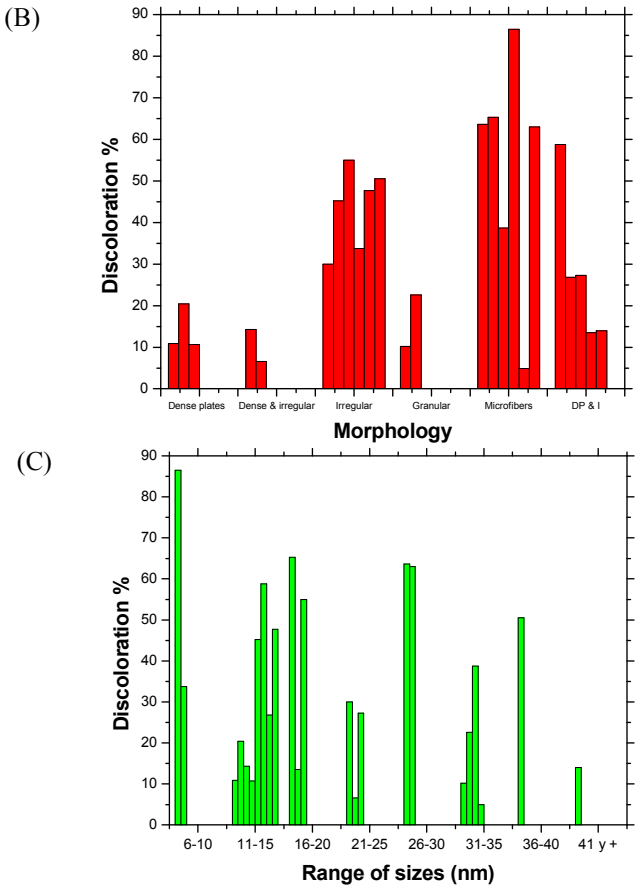

Figure 5. Graphical analysis of different parameters which are relevant for the photocatalytic properties. % discoloration as function of (A) phase, (B) morphology and (C) size.

Table 1. Crystal phases, sizes, morphologies and band gap of obtained TiO_2 nanostructures.

Photocatalyst	Temperature (°C)	Phase	Size (nm)	Dispersion	Band gap (eV)	Morphology
TiO_2-A-(I)p-500	500	Anatase	11.1	±0.1	3.7	Dense plates
TiO_2-M-(I)p-600	600	Mixture	12.9	±0.3	3.4	Dense plates
TiO_2-M-(I)p-700	700	Mixture	11.2	±0.5	3.6	Dense & irregular
TiO_2-R-(I)p-800	800	Rutile	24.3	±1.7	3.4	Irregular
TiO_2-A-(II)p-500	500	Anatase	12.8	±0.1	3.4	Dense plates
TiO_2-A-(II)p-600	600	Anatase	24.6	±9.5	3.3	Dense & irregular
TiO_2-A-(II)p-700	700	Anatase	32.5	±3.3	3.2	Granular
TiO_2-M-(II)p-800	800	Mixture	33.1	±2.0	3.3	Granular
TiO_2-A-(III)p-500	500	Anatase	27.1	±1.1	3.3	Microfibers
TiO_2-A-(III)p-600	600	Anatase	17.3	±4.9	3.4	Microfibers
TiO_2-A-(III)p-700	700	Anatase	32.3	±1.8	3.3	Microfibers
TiO_2-A-(III)p-800	800	Anatase	6.9 and 31.9	±0.2 and ±2.2	3.7	Microfibers
TiO_2-A-(IV)p-500	500	Anatase	11.1	±0.2	3.5	Irregular
TiO_2-A-(IV)p-600	600	Anatase	19.7	±1.3	3.4	Irregular
TiO_2-M-(IV)p-700	700	Mixture	35.1	±1.1	3.4	Microfibers
TiO_2-M-(IV)p-800	800	Mixture	30.3	±0.2	3.4	Microfibers
TiO_2-A-(V)p-500	500	Anatase	11.8	±0.7	3.5	Dense plates & irregular
TiO_2-A-(V)p-600	600	Anatase	13.6	±0.6	3.4	Dense plates & irregular
TiO_2-M-(V)p-700	700	Mixture	24.7	±1.0	3.2	Dense plates & irregular
TiO_2-M-(V)p-800	800	Mixture	18.2	± 0.9	3.3	Dense plates & irregular
TiO_2-A-(VI)p-500	500	Anatase	7.9	±0.8	3.7	Irregular
TiO_2-M-(VI)p-600	600	Mixture	11.0	±0.4	3.6	Irregular
TiO_2-M-(VI)p-700	700	Mixture	38.6	±3.3	3.4	Irregular

TiO_2-R-(VI)p-800	800	Rutile	62.1	±1.7	3.2	Dense plates & irregular

A: Anatase; R: Rutile; M; Mixture of Anatase and Rutile crystal phases

Table 2. Kinetic data for the photodegradation process of MB with all TiO_2 systems obtained from (I)-(VI) precursors at different temperatures.

Photocatalyst	Apparent photodegradation rate constant k (10^{-2} min^{-1})	decoloration rate at 25 min η (%)	R^2 linear fit (%)
TiO_2-A-(I)p-500	0.40 ±0.04	10.9	93.9

TiO_2-M-(I)p-600	0.80 ±0.04	20.4	98.4
TiO_2-M-(I)p-700	0.06 ±0.03	14.3	98.0
TiO_2-R-(I)p-800	1.30 ±0.10	30.0	93.8
TiO_2-A-(II)p-500	0.40 ±0.04	10.7	91.9
TiO_2-A-(II)p-600	0.33 ±0.03	6.6	88.8
TiO_2-A-(II)p-700	0.40 ±0.02	10.2	97.6
TiO_2-M-(II)p-800	1.00 ±0.06	22.6	97.2
TiO_2-A-(III)p-500	3.90 ±0.20	63.6	96.9
TiO_2-A-(III)p-600	4.10 ±0.20	65.3	97.4
TiO_2-A-(III)p-700	2.00 ±0.06	38.7	99.2
TiO_2-A-(III)p-800	7.13 ±0.01	86.5	99.8
TiO_2-A-(IV)p-500	2.40 ±0.01	45.2	97.8
TiO_2-A-(IV)p-600	3.10 ±0.01	55.0	98.0
TiO_2-M-(IV)p-700	0.20 ±0.02	4.9	91.1
TiO_2-M-(IV)p-800	4.00 ±0.20	63.0	97.1
TiO_2-A-(V)p-500	3.40 ±0.10	58.8	99.1
TiO_2-A-(V)p-600	1.30 ±0.04	26.8	99.2
TiO_2-M-(V)p-700	1.30 ±0.09	27.3	96.4
TiO_2-M-(V)p-800	0.60 ±0.03	13.5	98.0
TiO_2-A-(VI)p-500	1.70 ±0.03	33.7	99.7
TiO_2-M-(VI)p-600	2.40 ±0.02	47.7	95.9
TiO_2-M-(VI)p-700	2.60 ±0.02	50.5	94.6
TiO_2-R-(VI)p-800	0.50 ±0.02	14.0	98.5
TiO_2 P25 (Degussa)	6.7 ±0.36	75.5	98.0

Table 3. State-of-the-art related to photocatalytic performances and key factors (crystal phase, size and morphology) of different TiO_2 materials to degrade organic water pollutants in comparison with our best photocatalyst.

Organic Water pollutant (concentration)	Photocatalyst (concentration)	Irradiation light	Reaction Kinetics	decoloration rate	irradiation time	Major observation
Methylene Blue, MB						
MB (1×10^{-5} M)	Our best system TiO_2 in anatase phase from precursor (III) at 800°C (1.0 g L^{-1})	Xe lamp (150W) with 340 nm cut-off filter, 330 nm> λ >680 nm	Pseudo first-order kinetic	86.5%	25 min	Up to 86% degradation was possible after 25 min of irradiation time to pH 6.5. The photocatalyst is composed by fused particles of anatase phase using a novel solid synthetic route.
MB (10ppm)	TiO_2 nanoparticles (2,5 g L^{-1})	UV Lamp fig (40W)	Langmuir-Hinshelwood Pseudo first-order kinetic	71%	60min	Fused anatase and rutile particles with hexagonal and rectangular morphologies obtained by facile and low-cost bio-inspired synthesis were achieved. The average diameter was 22 nm. These systems were evaluated to degrade cationic dyes with an efficient photochemical response.[60]
MB (50ppm)	TiO_2 nanofibers	Xenon lamp UV-Vis (150W) with AM 1.5 G filter λ>400nm	NM	100%	180min	TiO_2 nanofibers were synthetized by electrospinning method and then a calcination treatment from 450-700°C was carry out. They studied the impact of calcination temperature on photocatalytic response, finding that the main factors involved in a better degradation of MB were particles size of nanofibers and defect

						density of anatase.[61]
MB (10mg L^{-1})	TiO_2 nanotubes (0,16g L^{-1})	Xenon visible light source (500W)	NM	99.1%	40min	An increased surface area, narrowed band gap and separated charge carriers were achieved in a defective TiO_2 nanotube, showing an improved photocatalytic activity under visible irradiation.[62]
MB (0.01mM)	Mesoporous TiO_2 (0.17g L^{-1})	UV light irradiation with eight tubes with a power source of 6 W , λ= 365 nm	NM	85%	60min	TiO_2 fused nanoparticles in anatase phase, with sizes of 10-20 nm obtained through a facile hydrothermal method for efficient photodegradation of MB.[63]
MB ($0.75x10^{-5}$M)	Hollow Titania Microspheres (HTS)	UV lamp 15W	Pseudo first-order kinetic	53%	90min	Hierarchical assembly, crystallinity, and surface chemistry of TiO_2 materials were controlled. Specially, an exposed {001} facets and designed surface chemistry were correlated to photocatalytic degradation of azo molecules.[64]
MB (1 mM)	TiO_2 nanoparticles	black light lamp (1mW)	NM	45%	20min	Quantitative determination of particle size and phase composition of TiO_2 nanoparticles on the photocatalytic properties.[65]
Other similar organic water pollutants						
Malachite green, MG (10ppm)	TiO_2 nanoparticles	UV Lamp	Langmuir-Hinshelwood Pseudo first-	78%	60 min	The same parameters were used with MB in this study. The photo-response allow an

	(2,5 g L^{-1})	(40W)	order kinetic			efficient degradation of both cationic dyes at the same irradiation time and conditions.[60]
Rhodamine B, RhB and Methyl Orange MO (0.01 mM)	TiO_2 hollow tetragonal nanocone (0.1 g L^{-1})	Full-arc Xe lamp (300 W) with a cut-off filter, $\lambda > 420$ nm	NM	95.0% for RhB 90.7% for MO	30 min	The large exposed (101) facets of this TiO_2 in anatase phase has exhibited excellent photocatalytic activities due a high surface area.[66]
Bisphenol A BPA, (200μM)	TiO_2 powder, Degussa P25 (0.5 g L^{-1})	Xe arc lamp (300W) IR water filter and cut-off filter, $\lambda > 320$ nm	Pseudo first-order kinetic	75% for BPA	4 h	The degradation and mineralization studies was carried out to compare the photocatalytic performance of pure and fluorinated TiO_2. The better results were founded for pure TiO_2 in the case of mineralization.[67]
Acetaminophen, Ace (1.3 μM)	TiO_2 powder, Degussa P25 (NM)	UVA/LED lamps, λ_{max} = 366 nm	NM	100%	8 min	This decomposition study reported a controlled periodic illumination by UVA/LED lamps, which exhibited a greater performance compared to continuous illumination under the same conditions.[68]
RhB (NM)	TiO_2 Nanopowder (0.3 g L^{-1})	visible light λ >420 nm	NM	90	5 h	TiO_2 nanopowder obtained by thermal plasma synthesis enhances the photocatalytic performance to degrade RhB under visible light.[69]

Methyl orange 50 mL, 4×10^{-5}M	TiO_2 powder (10mg)	Xe Lamp 300W	NM	90%	3h	The morphology, size, and phase of the anatase and rutile TiO_2 mesoporous single crystals were controlled by the hydrothermal synthetic way.[36]

NM:not mentioned

TABLE OF CONTENTS GRAPHIC